Supplemental Material

Supplemental Fig. S1

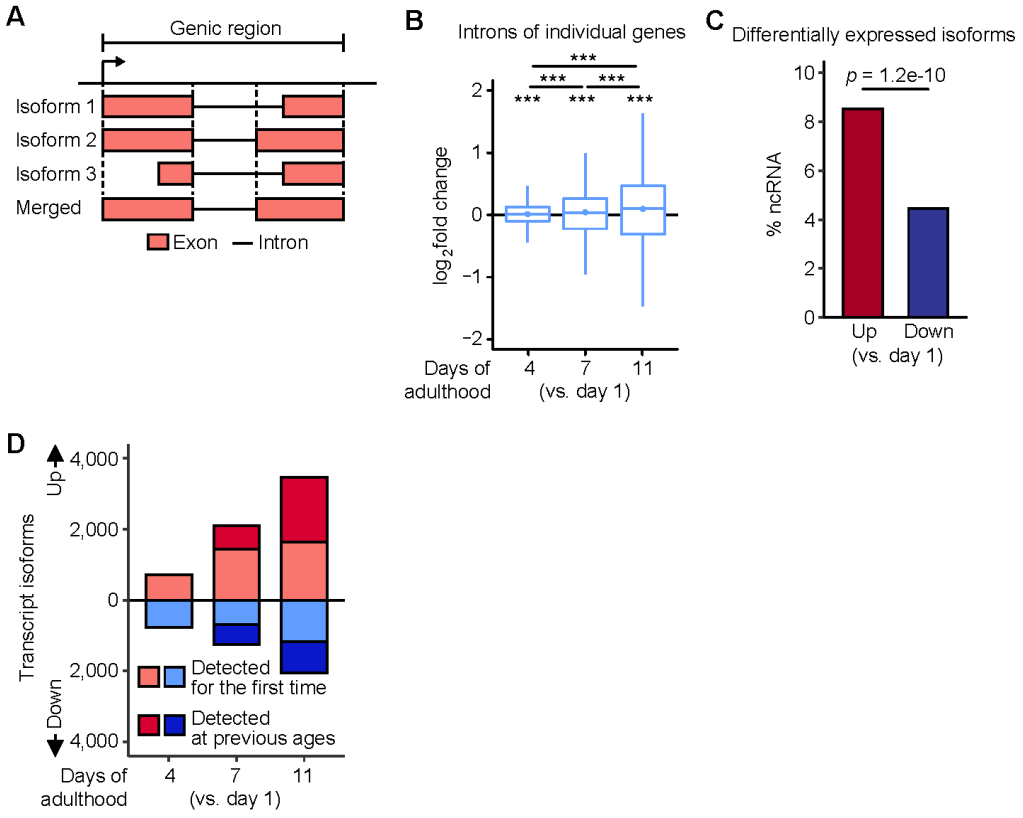

Supplemental Fig. S1. *Caenorhabditis elegans* transcriptome changes during aging. (***A***) Categorization of exons and introns in a genic region with multiple transcript isoforms. See Methods for detail. (***B***) Expression changes of intron regions in individual non-overlapping genes in aged wild-type animals. *p* values are indicated at the top, calculated by Wilcoxon signed rank test relative to day 1 of adulthood and two-tailed Wilcoxon rank sum exact test for other comparisons (***$p < 0.001$). (***C***) The proportion of noncoding RNAs (ncRNAs) in all transcripts that were up-regulated or down-regulated in aged animals. *p* value is shown at the top, calculated with two-tailed Fisher's exact test. (***D***) The number of transcript isoforms that were up-regulated and down-regulated in aged animals; 724, 2099, and 3467 transcripts

were up-regulated and 769, 1240, and 2045 transcripts were down-regulated in days 4, 7, and 11 of adult animals compared to those in day 1 adult animals. We speculate that these numbers of transcripts are sufficient to influence the physiology of organisms. Transcripts were chosen if absolute fold change > 2 and Benjamini and Hochberg-adjusted $p < 0.05$ relative to day 1 of adulthood.

Supplemental Fig. S2

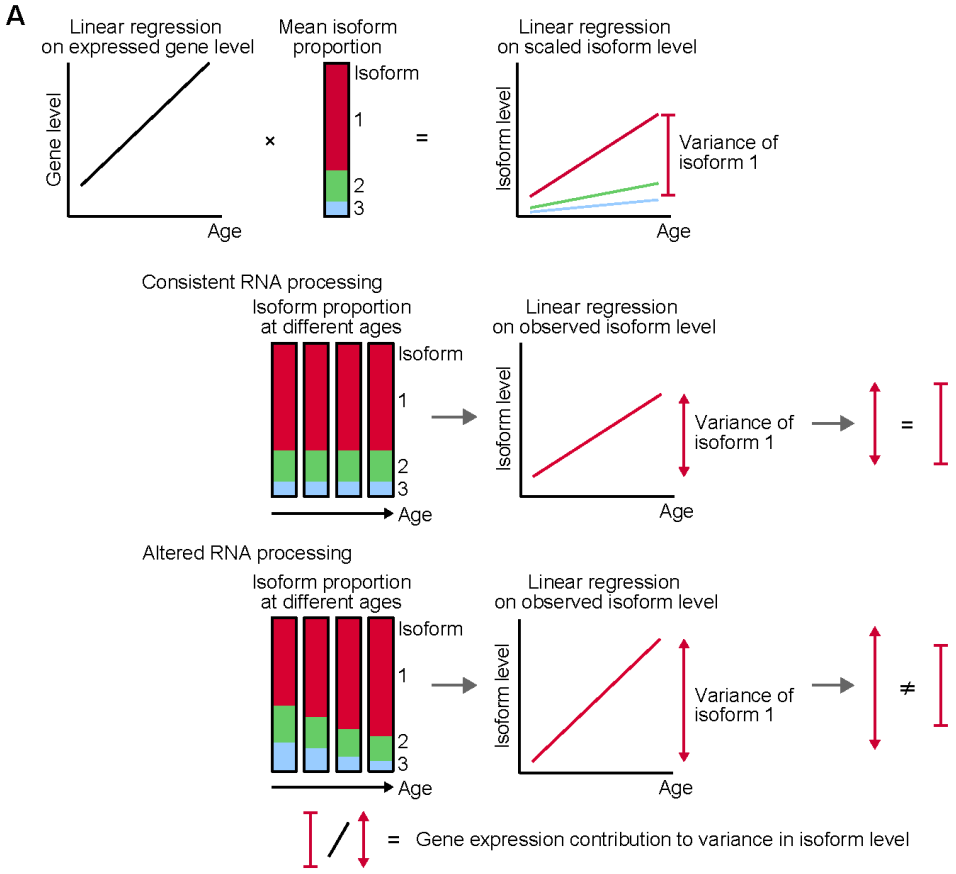

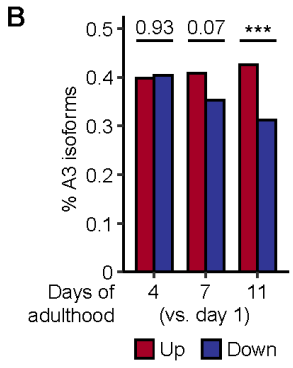

Supplemental Fig. S2. Aging up-regulates transcript isoforms containing distal alternative 3′ splice sites. (***A***) Schematic showing estimation of gene expression contribution to variance in isoform levels by using linear regression. If a gene has multiple isoforms, scaled isoform level is calculated by multiplying expressed gene level and mean isoform proportion at different ages. In this example, the gene has

three isoforms arbitrarily, and the first isoform (isoform 1) is used for interpretation. From the calculation, variance of isoform 1 was estimated. If RNA-processing events occur consistently at different ages, the variance of observed levels of the isoform will be the same as that of scaled levels. In contrast, if RNA-processing events are altered at different ages, the result of observed isoform levels will be different from that of scaled isoform levels. The ratio of variance by scaled isoform levels to that by observed isoform levels can be interpreted as the contribution of gene expression to variance in isoform levels. (***B***) The proportion of A3 isoforms in all transcript isoforms with the age-dependent up-regulation and down-regulation. *p* values are indicated on top, calculated by two-tailed Fisher's exact test (***$p < 0.001$).

Supplemental Fig. S3

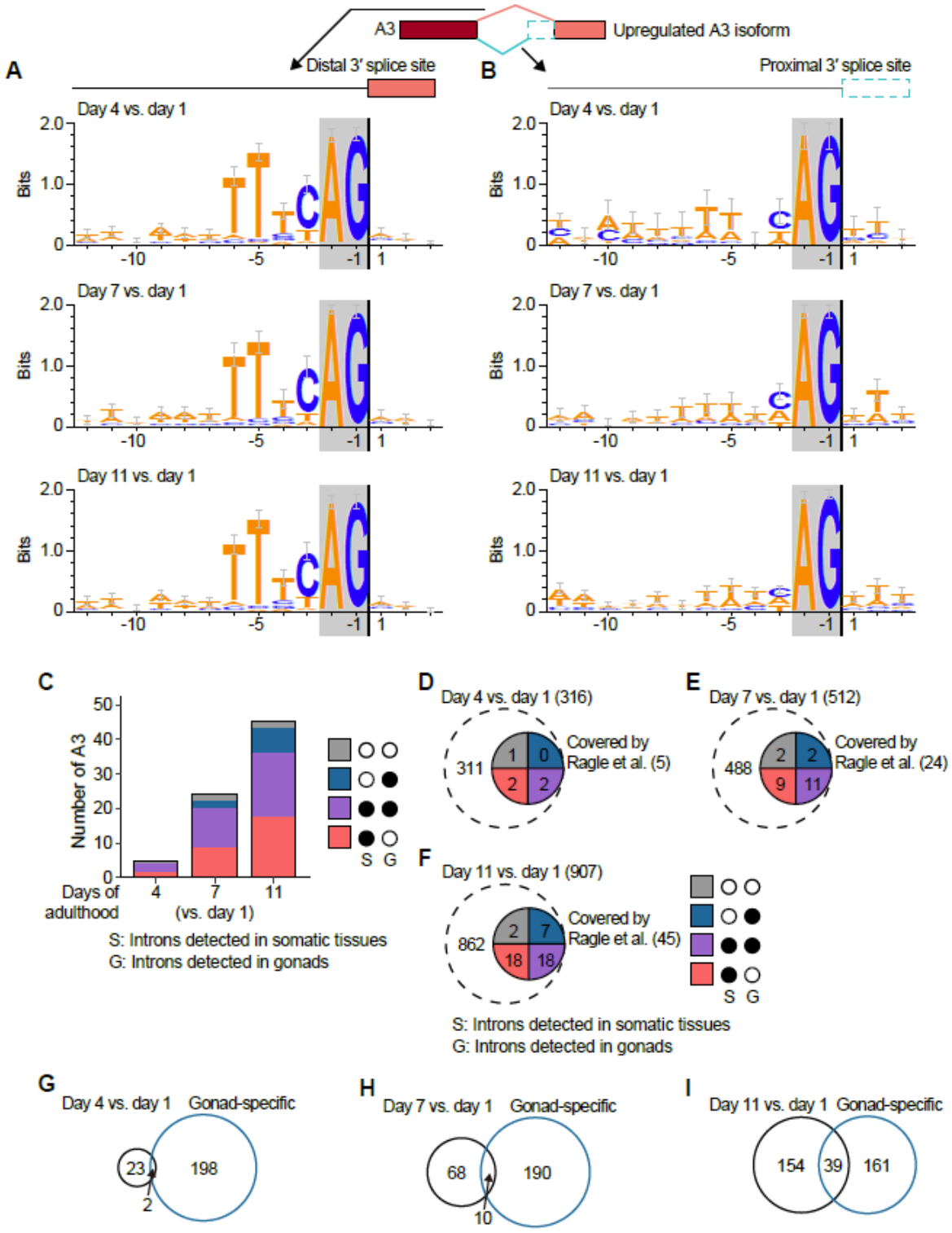

Supplemental Fig. S3. Age-dependent up-regulation of A3 isoforms occurs in somatic tissues as well as in gonads. (***A***, ***B***) Sequences around distal (***A***) and

proximal (***B***) 3′ splice sites in age-dependently up-regulated A3 isoforms with annotated junctions based on the meta-analysis of RNA sequencing data (Tourasse et al. 2017). Gray shaded boxes represent nucleotide positions at −2 to −1 from 3′ splice sites (+1). AG dinucleotides are the canonical 3′ splicing consensus motif. See Supplemental Fig. S4 for additional sequence analyses of the 3′ splice sites. (***C–F***) Comparisons between 5, 24 and 45 annotated introns with adjacent AG dinucleotides that are 6 nucleotides apart in A3 isoforms that were up-regulated respectively in day 4 (***D***), 7 (***E***), and 11 (***F***) adult animals and those detected in somatic tissues or gonads, obtained by reanalyzing a previous report (Ragle et al. 2015). A filled circle indicates a category that includes introns detected in somatic tissues (S) or introns detected in gonads (G). In particular, we found that 18 (40%) of 45 introns in A3 isoforms up-regulated in day 11 adult animals overlapped with those detected specifically in somatic tissues. (***G–I***) Comparisons between introns with adjacent AG dinucleotides that were within 18 nucleotides apart in A3 isoforms, which were up-regulated respectively in animals at day 4 (***G***), 7 (***H***), and 11 (***I***) of adulthoods and those detected specifically in gonads, obtained by reanalyzing data in a previous report (Ragle et al. 2015).

Supplemental Fig. S4

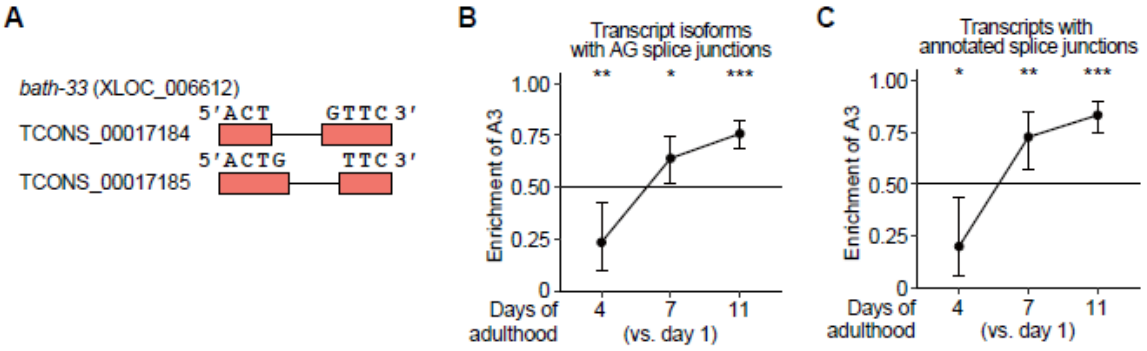

Supplemental Fig. S4. A subset of age-dependently up-regulated A3 isoforms contains consensus AG dinucleotides at both proximal and distal 3′ splice sites. (***A***) As an example, we analyzed the 3′ splice sites in *bath-33* transcripts, which raises the possibility that proximal and distal 3′ splice sites that were 1 nucleotide apart were alternative 5′ splice sites (Suzuki et al. 2022); the adjacent 3′ splice sites could be false positive cases of alternative 3′ splice sites. Note that 5′-ACT/GTTC-3′ was at the spliced exons of a transcript isoform (TCONS_00017184) in *bath-33* (XLOC_006612), and 5′-ACTG/TTC-3′ was at the spliced exons of another isoform (TCONS_00017185). (***B***) Analyses of 26, 83, and 205 junctions, which contained alternative 3′ splice sites within 18 nucleotides and AG dinucleotides at proximal and distal 3′ sites, of A3 isoforms that were up-regulated respectively in day 4, 7, and 11 of adult animals. The A3 usage was age-dependently increased in the A3 isoforms. (***C***) Analyses of A3 transcript isoforms annotated in meta-analysis of RNA-seq data (Tourasse et al. 2017). The annotated A3 isoforms covered 8.3%, 12.3%, and 13.9% of proximal 3′ splice sites and 32.9%, 37.6%, and 34.0% of distal 3′ splice sites in A3 isoforms up-regulated at day 4, 7, and 11 of adulthoods compared with those at day 1 adulthood. The A3 usage was age-dependently increased in the annotated A3 isoforms. These data indicate that adjacent 3′ splice

73 sites separated by 1 nucleotide apart did not change our conclusion regarding age-
74 dependent changes in A3 isoforms.

Supplemental Fig. S5

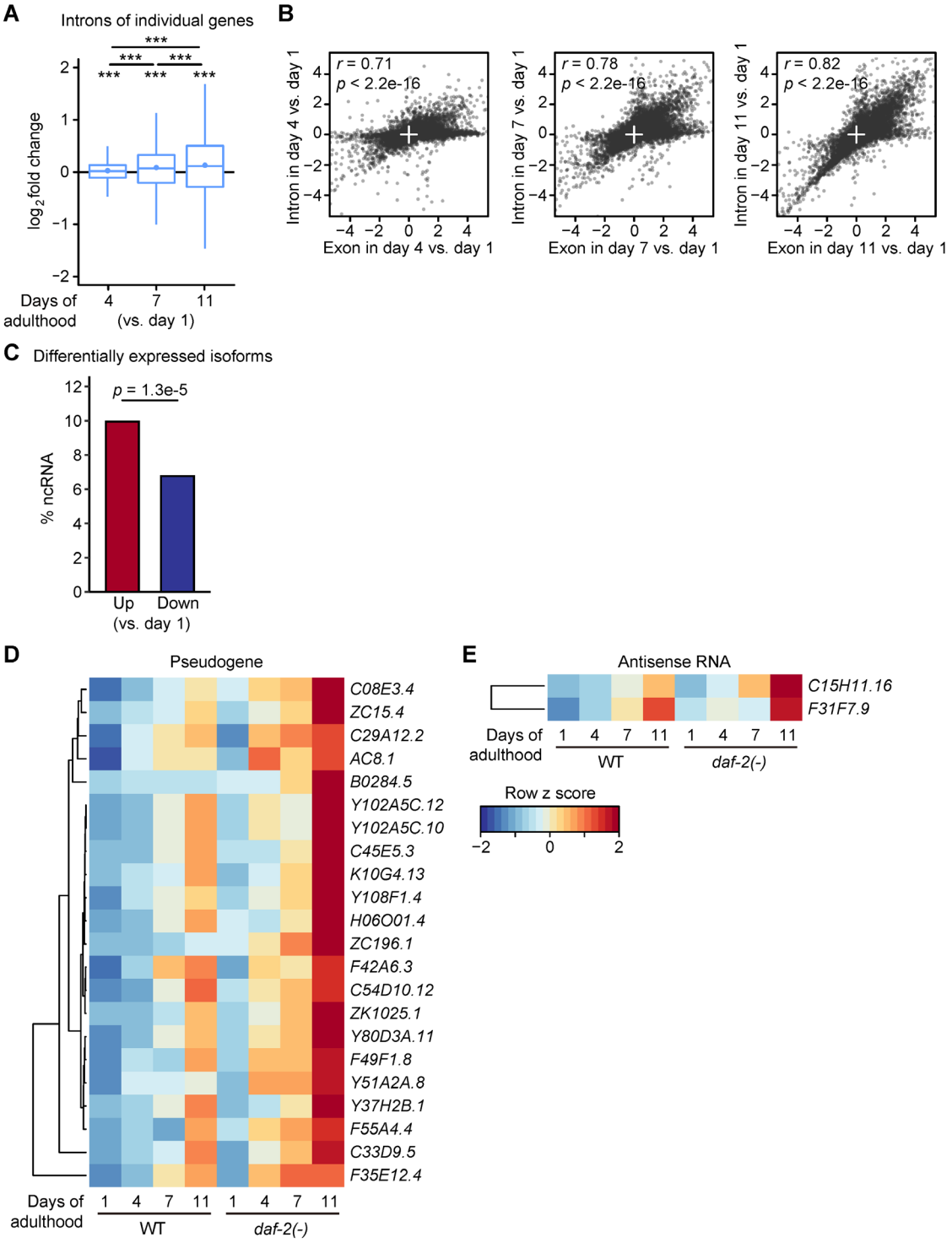

Supplemental Fig. S5. Reduced transcriptional fidelity is pervasive during aging in *daf-2* mutant animals. (***A***) Expression changes of intron regions in

individual non-overlapping genes in aged *daf-2(e1370)* [*daf-2(-)*] animals. *p* values are indicated on top, calculated by Wilcoxon signed rank test relative to day 1 of adulthood and two-tailed Wilcoxon rank sum exact test for other comparisons (***$p < 0.001$). (***B***) Comparisons between age-dependent expression changes in exon and intron regions in individual non-overlapping genes in *daf-2(-)* animals. Pearson correlation coefficient *r* and *p* value are shown. (***C***) The proportion of noncoding RNAs (ncRNAs) in all transcripts that were up-regulated or down-regulated in aged *daf-2(-)* animals. Transcripts were chosen if absolute fold change > 2 and Benjamini and Hochberg-adjusted $p < 0.05$ relative to day 1 of adulthood. *p* values are shown at the top, calculated by two-tailed Fisher's exact test. (***D***, ***E***) Relative expression levels of 22 pseudogene-coded RNAs (pseudogene) (***D***) and two antisense RNAs (***E***) matching the temporal shift at an individual transcript level in different ages of wild-type (WT) and *daf-2(-)* animals. Genes were chosen if fold change > 1 and $p < 0.05$ relative to day 1 of adulthood in WT animals, fold change > 2 and $p < 0.05$ relative to day 1 of adulthood for *daf-2(-)* animals, and fold change in *daf-2(-)* animals > that in WT animals at days 1 and 11 of adulthood. Differentially expressed snoRNA was not identified because of their variable levels.

Supplemental Fig. S6

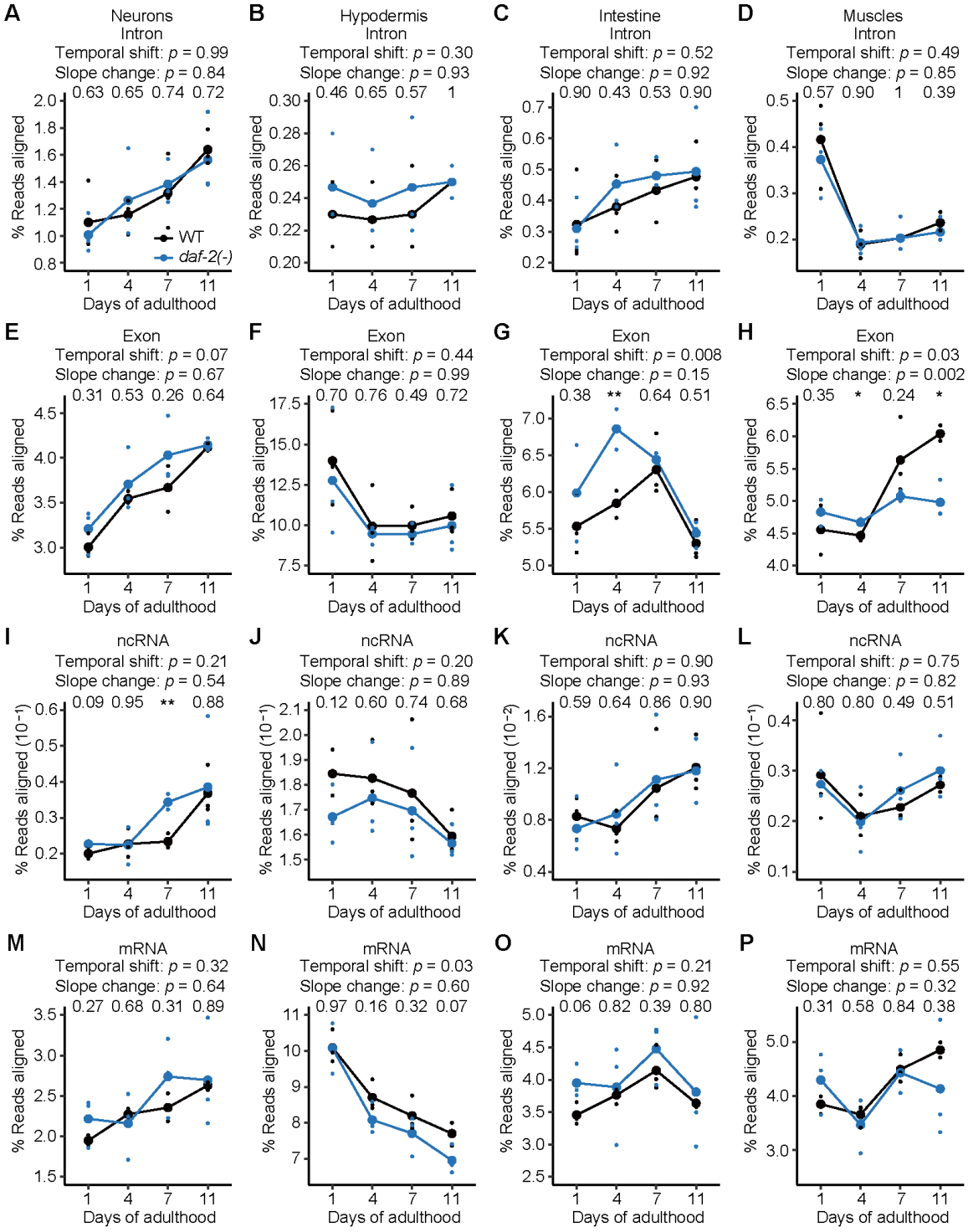

Supplemental Fig. S6. Age-dependent expression changes in most structural and functional transcripts match chronological aging in neurons and the

intestine. (***A–H***) Overall expression levels of structural elements, including intron (***A–D***), and exon regions (***E–H***), enriched in neurons (***A***, ***E***), the hypodermis (***B***, ***F***), the intestine (***C***, ***G***), and the muscles (***D***, ***H***), in wild-type (WT) and *daf-2(e1370)* [*daf-2(-)*] animals at indicated ages. (***I–P***) Overall levels of functional RNA elements, including noncoding RNA (ncRNA) (***I–L***) and protein-coding messenger RNA (mRNA) (***M–P***), enriched in neurons (***I***, ***M***), the hypodermis (***J***, ***N***), the intestine (***K***, ***O***), and the muscles (***L***, ***P***), in WT and *daf-2(-)* animals at indicated ages. The levels of transcripts enriched in a specific tissue were significantly higher than the average levels across all the other tissues (fold change > 2 and adjusted *p* value < 0.05) (Kaletsky et al. 2018). *p* value is shown at each day, calculated by two-tailed Welch's *t*-test between WT and *daf-2(-)* animals of the same chronological age. In each panel, two *p* values are shown for the effects of genotypes on transcript levels that correspond to "Temporal shift", and those for interaction between genotypes and ages that correspond to "Slope change", calculated by using two-way analysis of variance (ANOVA).

Supplemental Fig. S7

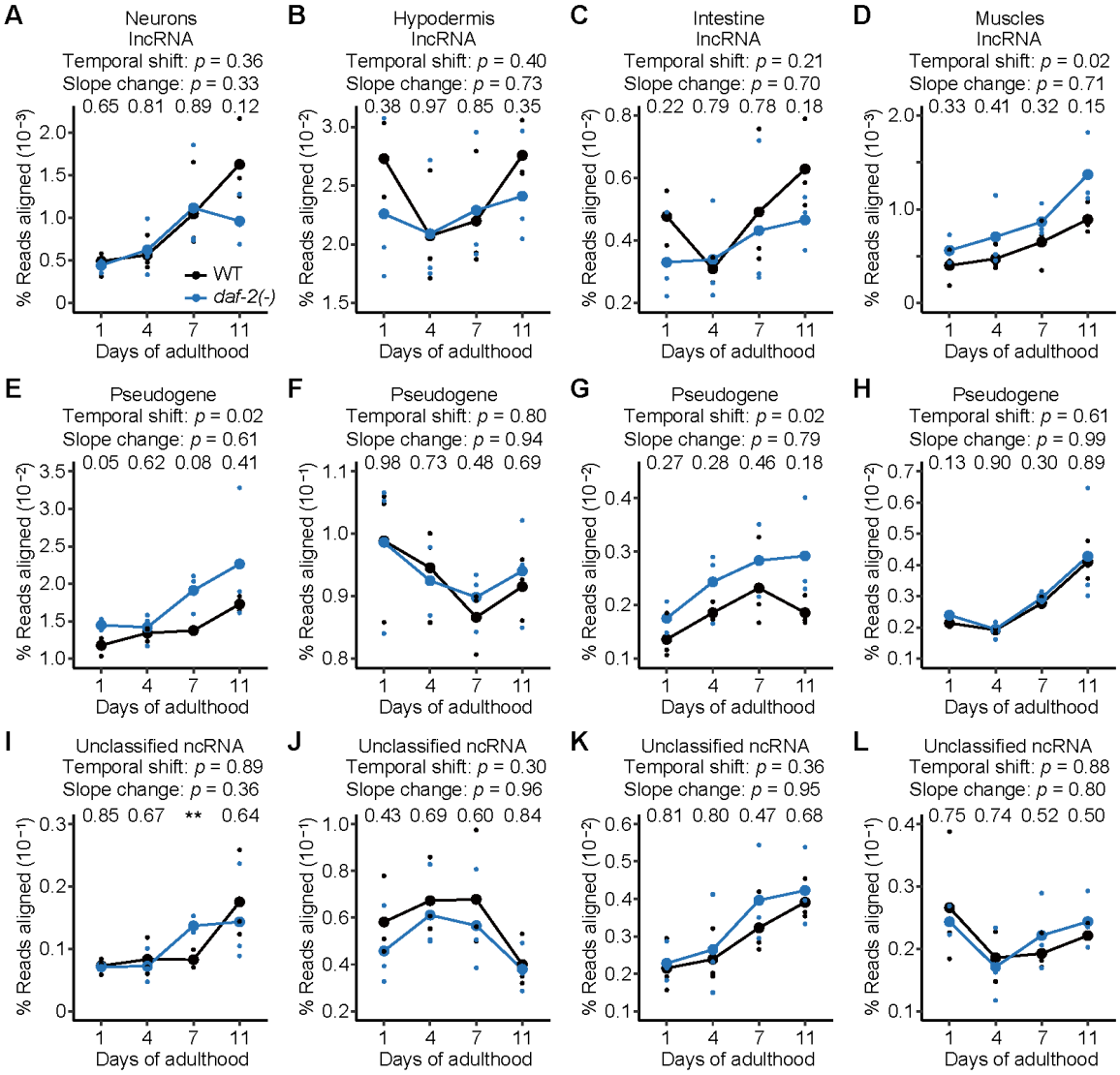

Supplemental Fig. S7. Age-dependent expression changes in most subcategories of ncRNAs match chronological aging in neurons and the intestine. Age-dependent level changes in noncoding RNA (ncRNA), including long ncRNA (lncRNA) (***A–D***), pseudogene-coded RNA (pseudogene) (***E–H***), and unclassified ncRNA (***I–L***), enriched in neurons (***A***, ***E***, ***I***), the hypodermis (***B***, ***F***, ***J***), the intestine (***C***, ***G***, ***K***), and the muscles (***D***, ***H***, ***L***), in wild-type (WT) and *daf-2(e1370)* [*daf-2(-)*] animals at indicated ages. snoRNAs, snRNAs, or antisense RNAs were not

analyzed because of insufficient read depth. The levels of transcripts enriched in a specific tissue were significantly higher than the average levels across all the other tissues (fold change > 2 and adjusted *p* value < 0.05) (Kaletsky et al. 2018). *p* value is shown at each day, calculated by two-tailed Welch's *t*-test between WT and *daf-2(-)* animals of the same chronological age (**$p < 0.01$). In each panel, two *p* values are shown for the effects of genotypes on transcript levels that correspond to "Temporal shift", and those for interaction between genotypes and ages that correspond to "Slope change", calculated by using two-way analysis of variance (ANOVA).

Supplemental Fig. S8

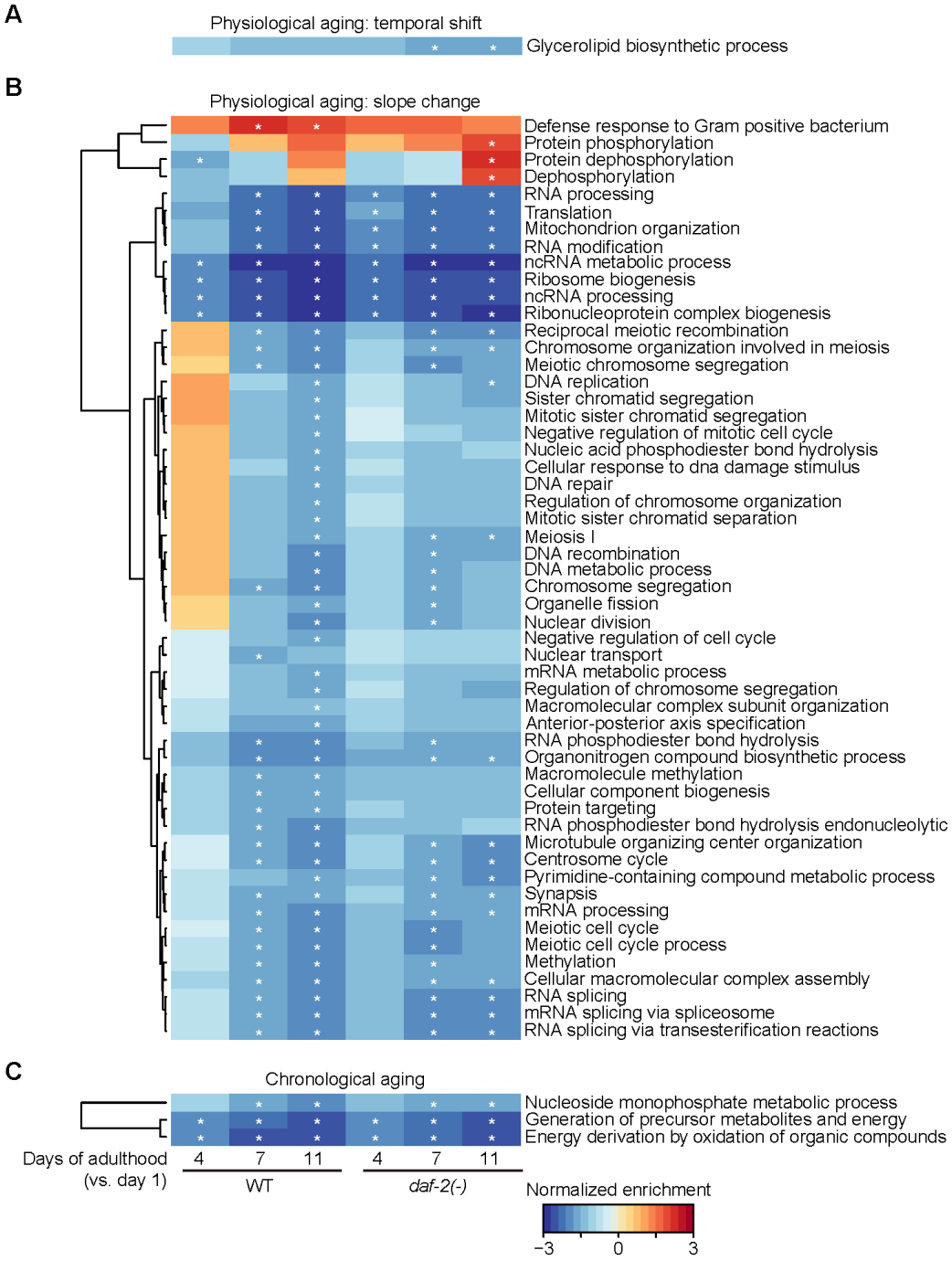

Supplemental Fig. S8. Biological processes associated with physiological aging and chronological aging. (***A–C***) Normalized enrichment of expression changes of genes related to particular biological processes in wild-type (WT) and *daf-2* mutant [*daf-2(-)*] animals during aging. The changes of the processes were

associated with physiological aging, which include temporal shift (***A***) and slope change (***B***), and chronological aging (***C***). Adjusted *p* value is shown in each cell, calculated by gene set enrichment analysis test and adjusted using false discovery rates (*adjusted $p < 0.1$).

Supplemental Fig. S9

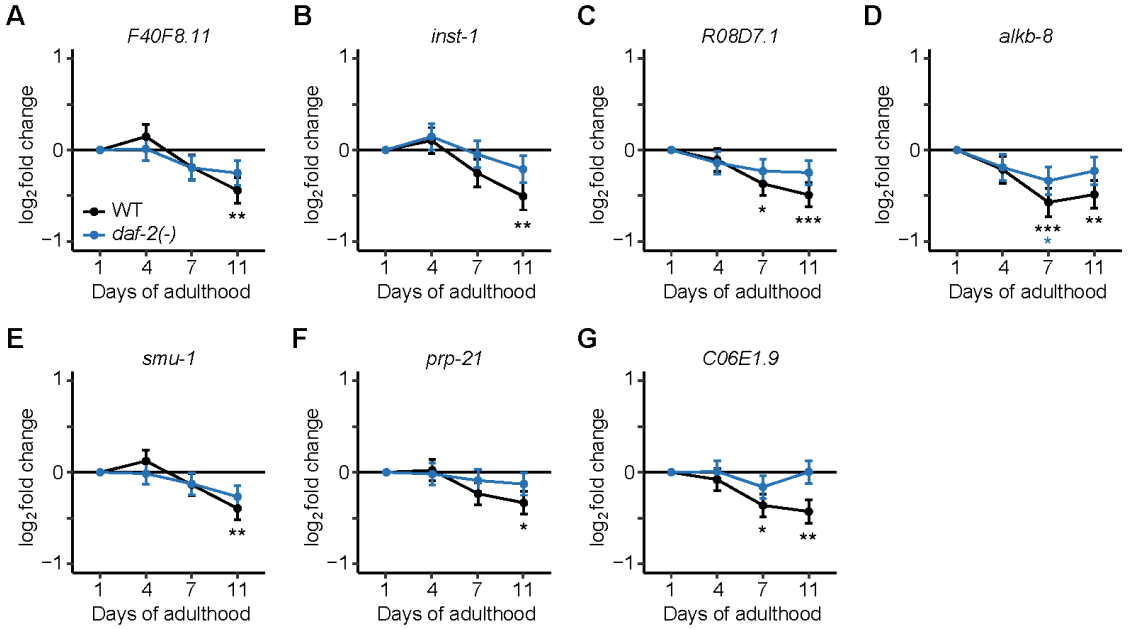

Supplemental Fig. S9. *daf-2* mutations slow age-dependent down-regulation of various genes encoding RNA-processing components. (***A–G***) Expression changes of the RNA-processing component-encoding genes, *F40F8.11* (***A***), *inst-1* (***B***), *R08D7.1* (***C***), *alkb-8* (***D***), *smu-1* (***E***), *prp-21* (***F***), and *C06E1.*9 (***G***), during aging in wild-type (WT) and *daf-2(e1370)* [*daf-2(-)*] animals. Adjusted *p* values are shown, calculated by using DESeq2's Wald test relative to day 1 adult and adjusted by using the procedure of Benjamini and Hochberg (*adjusted $p < 0.05$, **adjusted $p < 0.01$, ***adjusted $p < 0.001$).

Supplemental Fig. S10

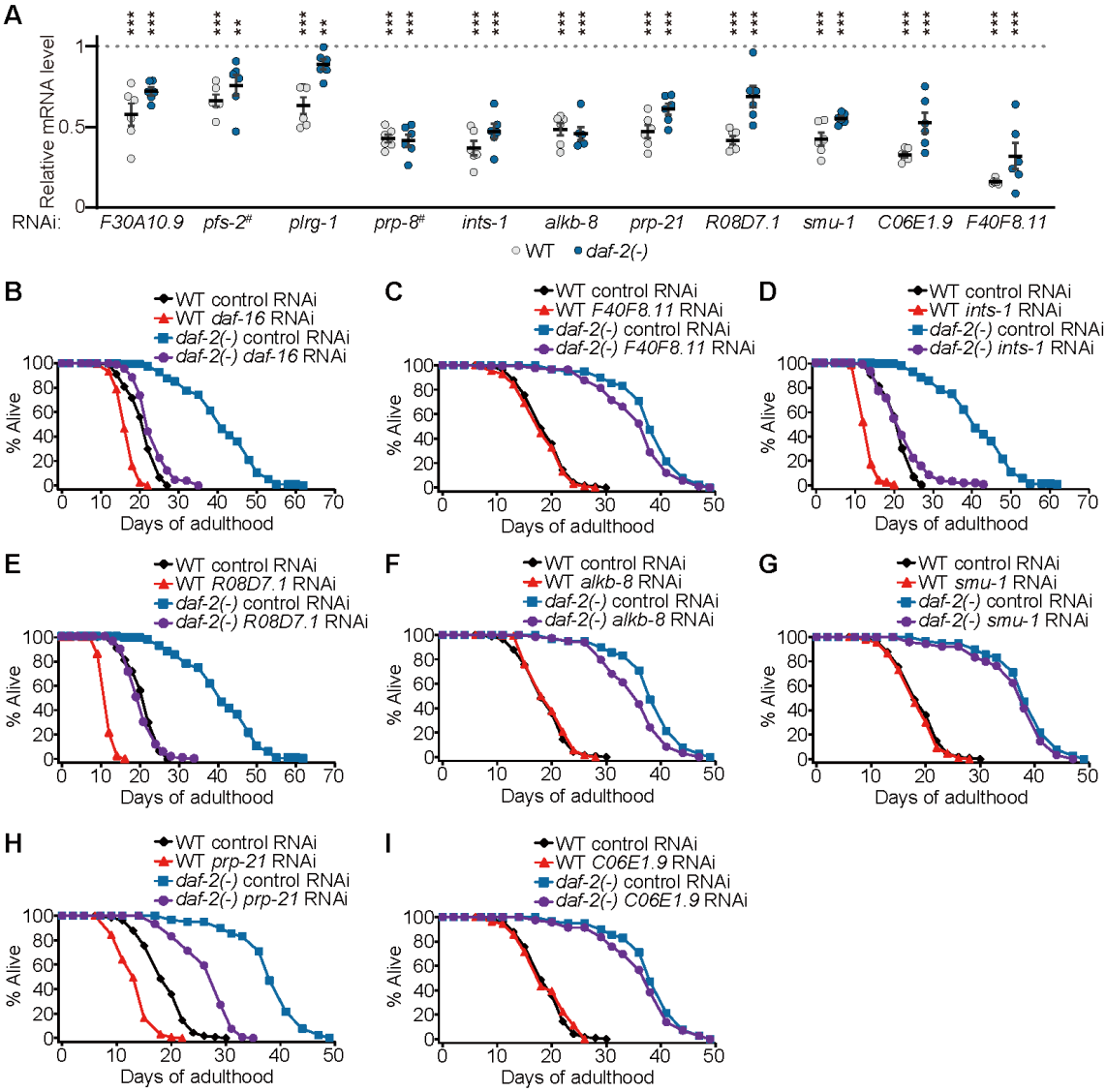

Supplemental Fig. S10. The effects of RNAi targeting each of the tested genes encoding RNA-processing components. (***A***) RNAi efficiency for indicated target genes in wild-type (WT) and *daf-2(e1370)* [*daf-2(-)*] animals measured by using qRT-PCR (n = 6 for each condition). Error bars represent standard error of the mean (SEM). *p* values are shown at the top, calculated by two-tailed Student's *t*-test relative to control RNAi (**$p < 0.01$, ***$p < 0.001$). Whole-life RNAi treatment was used except those noted with sharp (#) signs, which were performed using adult-only

RNAi treatment. (***B–I***) Lifespan curves of WT and *daf-2(-)* animals treated with control RNAi and RNAi against *daf-16* (a positive control) (***B***), *F40F8.11* (***C***), *ints-1* (***D***), *R08D7.1* (***E***), *alkb-8* (***F***), *smu-1* (***G***), *prp-21* (***H***), or *C06E1.9* (***I***) (N ≥ 90 for each condition). See Source files for additional repeats and statistical analysis for the lifespan data shown in this figure.

Supplemental Fig. S11

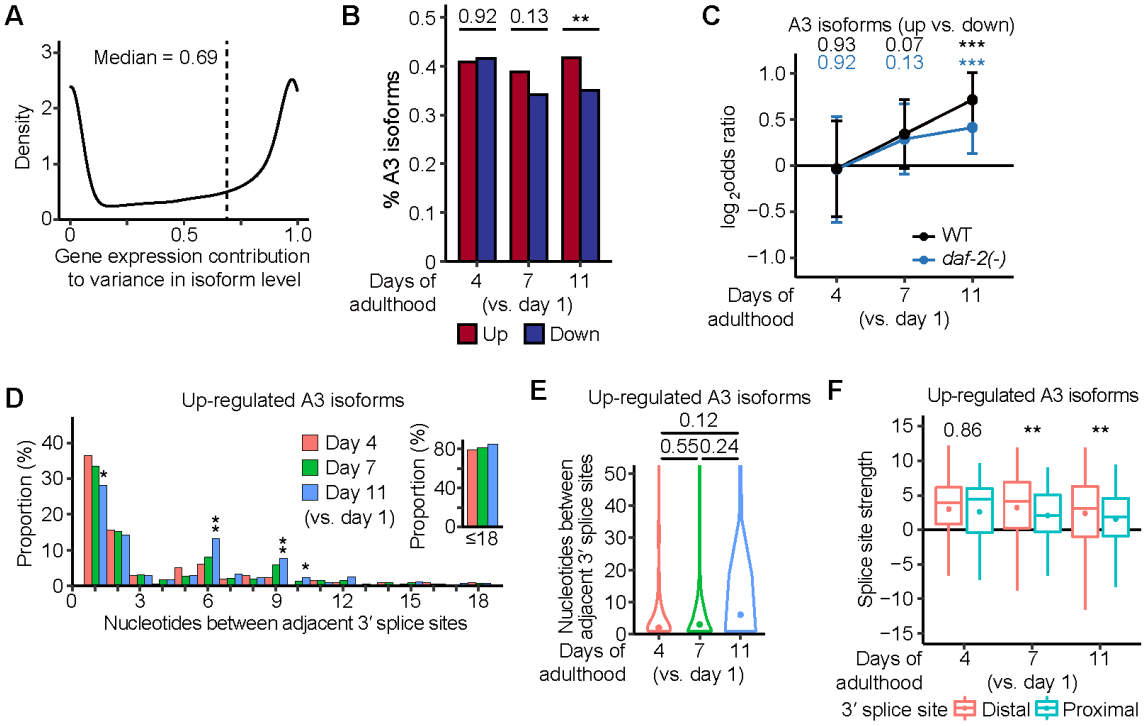

Supplemental Fig. S11. *daf-2* mutations delay age-dependent changes in the proportion of A3 in transcript isoforms. (***A***) Gene expression contribution to variance in isoform levels in *daf-2(e1370)* [*daf-2(-)*] animals. See Fig. S2A for a schematic overview. (***B***) The proportions of A3 isoforms in all transcript isoforms with age-dependent up-regulation and down-regulation in *daf-2* mutants. *p* values are indicated at the top, calculated by two-tailed Fisher's exact test (***$p < 0.001$). (***C***) Odds ratio between A3 isoforms displaying age-dependent up-regulation and those exhibiting down-regulation. Adjusted *p* values are shown at the top, calculated by two-tailed Fisher's exact test (***adjusted $p < 0.001$). (***D***) Nucleotides between adjacently located proximal and distal 3′ splice sites in age-dependently up-regulated A3 isoforms in *daf-2(-)* animals. Inset: proportion of the cases with adjacent 3′ splice sites located within 18 nucleotides. *p* values are shown at the top, calculated by two-tailed Fisher's exact test (*$p < 0.05$, **$p < 0.01$, ***$p < 0.001$). (***E***) Distribution of

nucleotides between adjacent 3′ splice sites in age-dependently up-regulated A3 isoforms in *daf-2(-)* animals. *p* values are shown at the top, calculated using two-tailed Wilcoxon rank sum exact test. (***F***) Splice site strength of proximal and distal 3′ splice sites in age-dependently up-regulated A3 isoforms in *daf-2(-)* animals. The A3 isoforms were annotated by the meta-analysis of RNA-seq data (Tourasse et al. 2017). The strength was calculated based on a maximum entropy model. *p* values are indicated on top, calculated by using two-tailed Wilcoxon rank sum exact test (**$p < 0.01$).

Supplemental Fig. S12

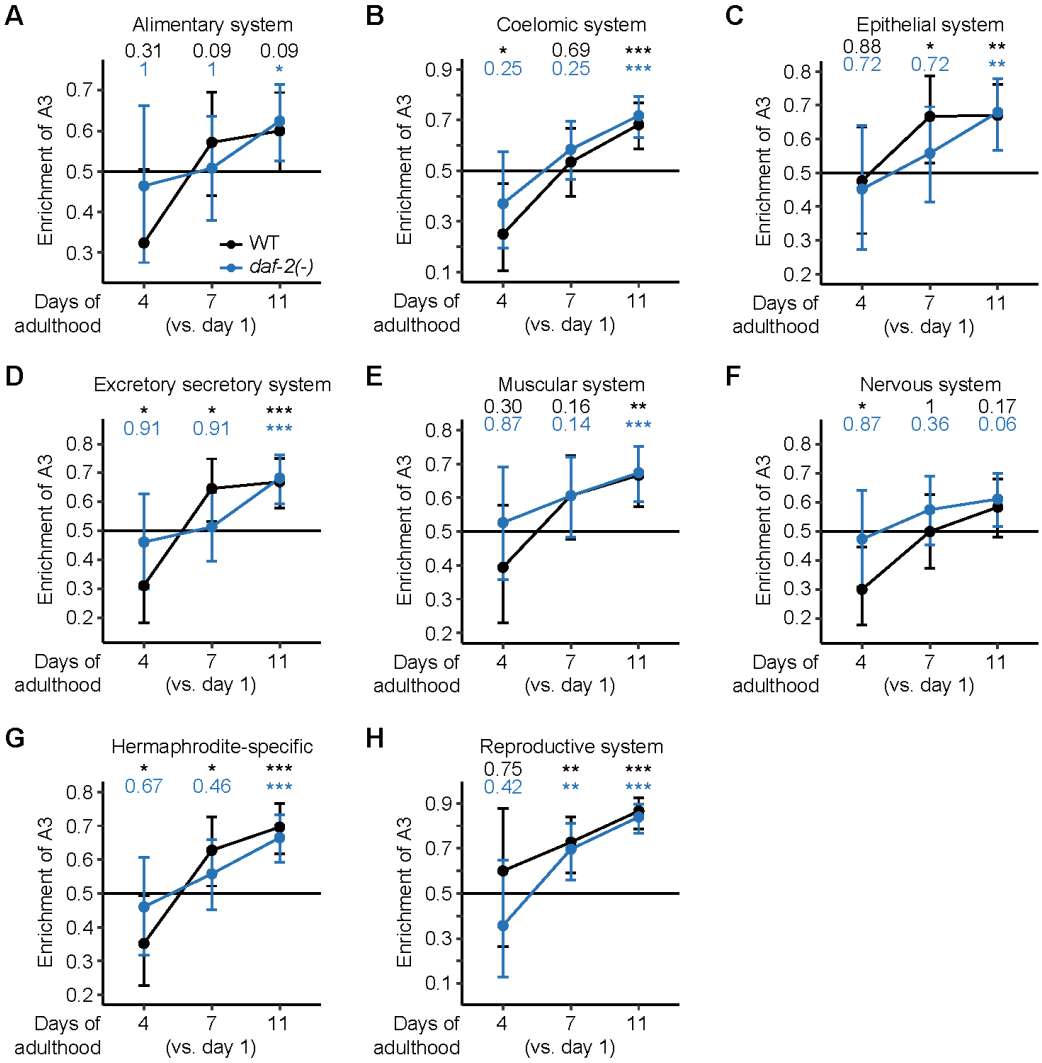

183

184 **Supplemental Fig. S12. *daf-2* mutations decelerate age-dependent increases in**
185 **the A3 usage in somatic tissues.** Enrichment of A3 in transcript isoforms that were
186 up-regulated among isoforms whose fractions changed during aging in alimentary
187 (***A***), coelomic (***B***), epithelial (***C***), excretory secretory (***D***), muscular (***E***), nervous (***F***),
188 hermaphrodite-specific (***G***), and reproductive (***H***) systems (Kaletsky et al. 2018) in
189 wild-type (WT) and *daf-2(e1370)* [*daf-2(-)*] animals**.** Adjusted *p* values are shown at
190 the top, calculated by one-proportion z-test and adjusted using false discovery rates
191 (*adjusted $p < 0.1$, **adjusted $p < 0.01$, ***adjusted $p < 0.001$). *daf-2* mutations

192 decreased the slope of the age-dependent increase in A3 or delayed the increase in
193 A3 in genes enriched in somatic tissues, but not in reproductive system.

Supplemental Fig. S13

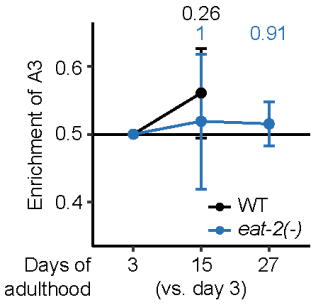

Supplemental Fig. S13. Dietary restriction mimetic *eat-2* mutations tend to slow age-dependent increases in the A3 usage. The enrichment of A3 in transcript isoforms that were up-regulated among isoforms whose fractions changed during aging in wild-type (WT) and *eat-2(ad1116)* [*eat-2(-)*] animals (Heintz et al. 2017). Adjusted *p* values are shown at the top, calculated by one-proportion z-test and adjusted using false discovery rates. Because of a relatively large variance among samples (confidential interval = 0.13), WT animals exhibited marginal age-dependent increases in A3 at day 15 of adulthood compared with day 3 of adulthood (p = 0.26). Nevertheless, A3 did not exhibit significant changes in *eat-2(-)* mutants until day 27 of adulthood (CI = 0.20 and p = 1 in day 15, CI = 0.06 and p = 0.91 in day 27).

Supplemental Fig. S14

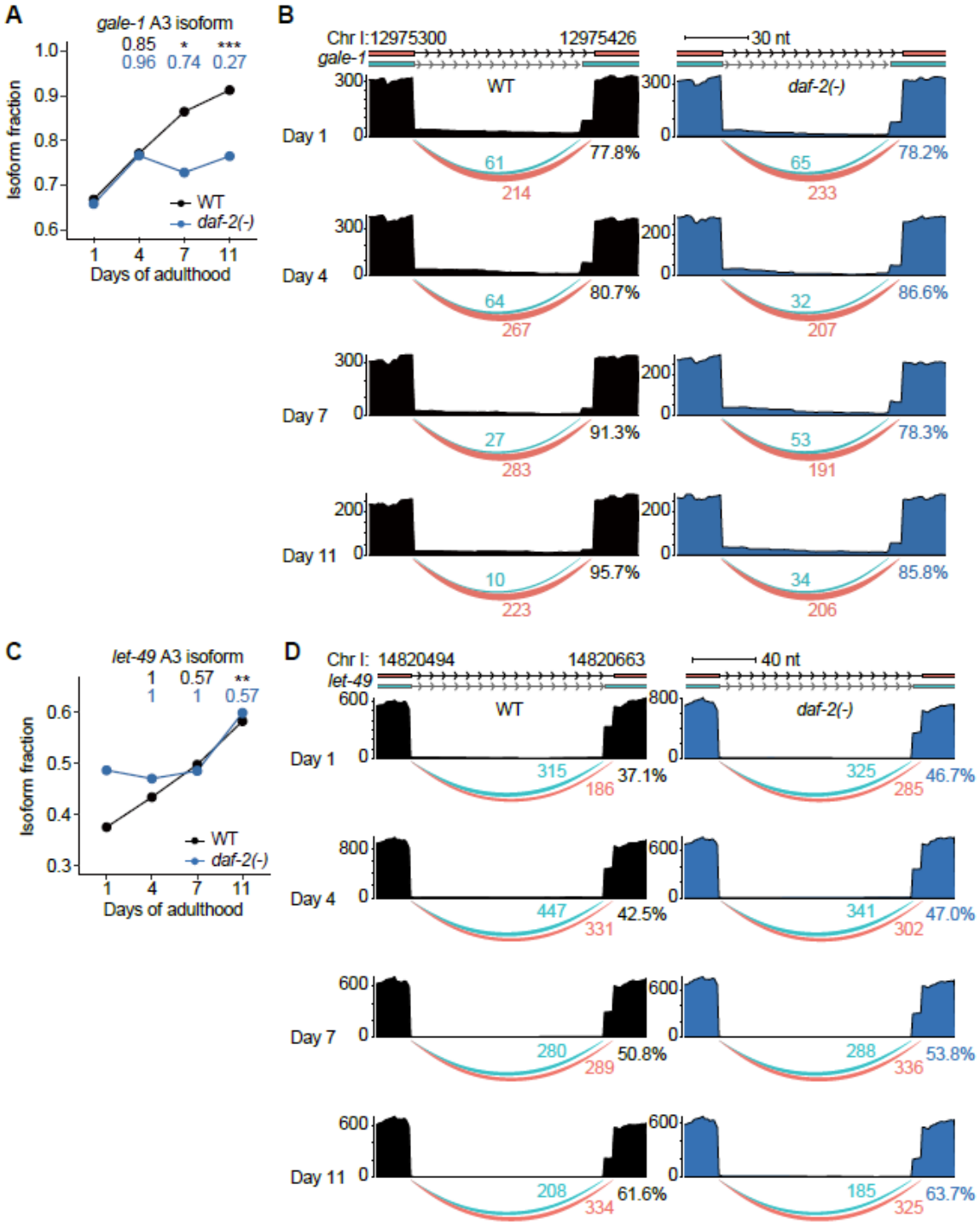

Supplemental Fig. S14. *daf-2* mutations slow age-dependent increases in the usage of distal 3′ splice sites in *gale-1* and *let-49* A3 isoforms. (***A***, ***C***) Changes in isoform fraction of *gale-1* (***A***) and *let-49* (***C***) A3 isoforms during aging in wild-type

(WT) and *daf-2(e1370)* [*daf-2(-)*] animals. Adjusted *p* values are shown at the top, calculated relative to day 1 of adulthood data using IsoformSwitchAnalyzeR (**adjusted $p < 0.01$). (***B, D***) Aligned reads (top) and junction usage (bottom) of *gale-1* (Chr I: 12975300–12975426) (***B***) and *let-49* (Chr I: 14820494–14820663) (***D***) A3 isoforms in WT and *daf-2(-)* animals at indicated ages. Pink lines represent junctions with distal 3′ splice sites, whereas cyan lines represent those with proximal 3′ splice sites. Numbers below the lines indicate the numbers of reads aligned at the junctions. Percent numbers represent the ratios of reads at junctions with distal 3′ splice sites to total reads at junctions with proximal and distal 3′ splice sites.

Supplemental Fig. S15

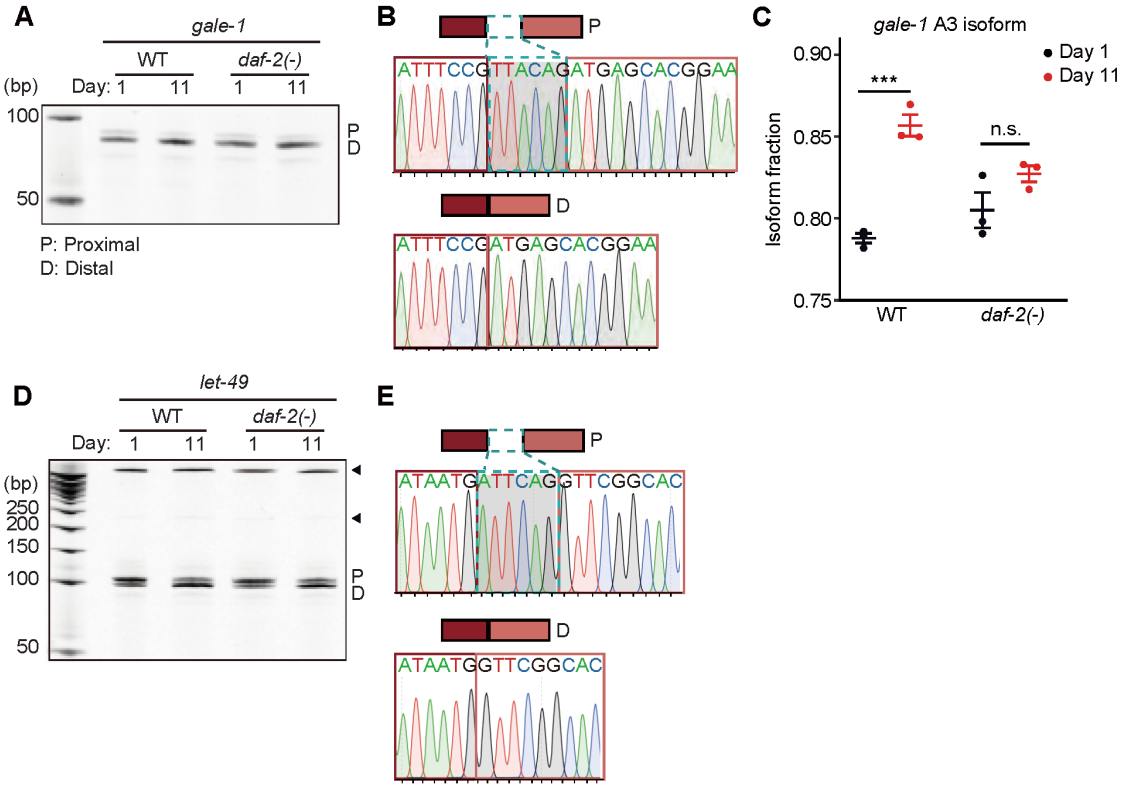

Supplemental Fig. S15. Verification of the down-regulation of age-dependent increases in the usage of distal 3′ splice sites in *gale-1* and *let-49* A3 isoforms by *daf-2* mutations. (***A***) RT-PCR analysis of the proximal (P) and distal (D) splice sites of *gale-1* isoforms at days 1 and 11 of adulthoods. (***B***) Sequences and electropherograms of RT-PCR amplicons of *gale-1* isoforms. (***C***) Isoform fraction of *gale-1* A3 isoforms that were obtained from three independent RT-PCR experiments. Error bars represent standard error of the mean (SEM). *p* values were calculated by using two-tailed Student's *t*-test relative to day 1 of adulthood data (***$p < 0.001$, n.s.: not significant). See Source files for statistical analysis of the RT-PCR data shown in this figure and Supplemental Table S4 for primer sequences used in this RT-PCR. (***D***) RT-PCR analysis of the P and D splice sites of *let-49* isoforms at days 1 and 11 of adulthoods. Arrowheads indicate nonspecific bands. (***E***) Sequences and

232 electropherograms of RT-PCR amplicons of *let-49* isoforms.

Supplemental Fig. S16

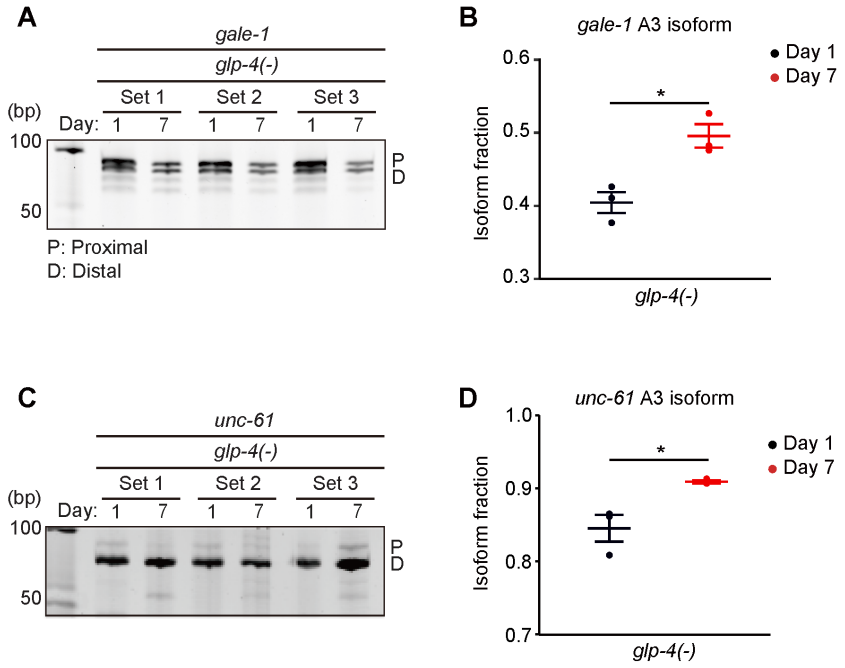

Supplemental Fig. S16. The age-dependent increases in the usage of distal 3′ splice sites in *gale-1* and *unc-61* A3 isoforms occur in germline-defective *glp-4* mutants. (***A***) RT-PCR analysis of the proximal (P) and distal (D) splice sites of *gale-1* isoforms in *glp-4(bn2ts)* [*glp-4(-)*] at days 1 and 7 of adulthoods. (***B***) Isoform fraction of *gale-1* A3 isoforms that were obtained from three independent RT-PCR experiments. (***C***) RT-PCR analysis of the P and D splice sites of *unc-61* isoforms in *glp-4(-)* mutants at days 1 and 7 of adulthoods. (***D***) Isoform fraction of *unc-61* A3 isoforms that were obtained from three independent RT-PCR experiments. Error bars represent standard error of the mean (SEM). *p* values were calculated by using two-tailed Student's *t*-test relative to day 1 adulthood data (*$p < 0.05$. See Source files for statistical analysis of the RT-PCR data shown in this figure and Supplemental Table S4 for primer sequences used in this RT-PCR).

Supplemental Table S1. Age-dependently regulated transcripts associated with physiological or chronological aging.

Supplemental Table S2. Age-dependently regulated gene ontology terms associated with physiological or chronological aging.

Supplemental Table S3. A3 isoforms that were differentially regulated in wild-type and *daf-2* mutant animals in old age compared with those at day 1 of adulthood.

Supplemental Table S4. List of RT-PCR primers used in this study.